International Journal of Enhanced Research in Science Technology & Engineering, ISSN: 2319-7463
Vol. 3 Issue 6, June-2014, pp: (407-422), Impact Factor: 1.252, Available online at: www.erpublications.com

A numerical study of turbulent flame speed models for H_2/CH_4/Air premixed combustion

Mark Tidswell[1], Dr. Siva Muppala[2]
[1,2]School of Mechanical and Automotive Engineering, Faculty of Science Engineering and Computing, Kingston University, London

Abstract: This study has assessed the validity of the commercially available turbulent flame speed models within ANSYS Fluent as applied to hydrogen/methane/air combustion, with 5 different fuel compositions considered from 100% methane to 100% hydrogen. It was found that existing turbulent flame speed models were capable of producing accurate predictions up to 60% hydrogen with the Zimont model being the best performing model. However beyond 60% hydrogen content the accuracy of the predictions degraded dramatically. As a result of this attempts were made to improve the results by tuning the Zimont turbulent flame speed constant, however this produced minimal improvement in the results. Finally a modification was developed and used in tandem with the exponential effective Lewis number term taken from literature, this elicited a significant improvement in the results at 80% and 100% hydrogen.

Nomenclature

c = Reaction progress variable
$\bar{c}$ = Average reaction progress variable
C_D= Coefficient of drag (0.37)
k = Turbulent kinetic energy (m^2/s^2)
l = Turbulence length scale (m)
l_{alg} = Algebraic flame brush thickness (m)
l_f = Flame brush thickness (m)
Sc = Reaction progress source term
Sc_i = Schmidt number of i^{th} species
Sc_t = Turbulent Schmidt number
ύ= RMS (root-mean-square) velocity (m/s)
U_l = Laminar flame speed (m/s)
U_o = Inlet velocity (18 m/s)
U_t= Turbulent flame speed (m/s)
Y = Species mass fraction

Latin/Greek symbols
α= Unburnt thermal diffusivity
λ = Thermal conductivity
ε = Turbulence dissipation rate
μ =Dynamic viscosity
ν = Kinematic viscosity
ν_η = Kolmogorov viscosity
τ_t= Turbulence time scale (s)
τ_{chem} = Chemical time scale (s)
ρ = Density

I. Introduction

Recently there have been significant efforts expended towards developing a feasible solution to address the need to reduce polluting emissions, but produce greater amounts of energy. To date lean premixed combustion has been the favoured approach to attain the lower temperatures required minimising the level of NOx production and therefore emissions; however this requires a delicate balancing act. Lean combustion is inherently unstable which can lead to localised extinction which in turn can cause the emission of unburnt-hydrocarbons, clearly an undesirable side effect. As flame extinction clearly has safety implications the typical level of NOx emissions currently being achieved is in the region of 25 ppm, it is expected that future regulations will require this to be further reduced. As hydrogen has a far higher burning velocity than methane, switching to hydrogen as a fuel would seem a logical step to address this stability issue and attain ultra-lean premixed combustion whilst burning an abundant 'green' fuel. However stable, low NOx combustion requires quick, consistent mixing of the fuel and air, which can pose a challenge with natural gas and is made even more challenging by hydrogens highly reactive and diffusive nature [1]. In addition to this the increased chance of flashback and the safety issues around storing and distributing hydrogen makes this non-feasible. A possible step towards pure hydrogen combustion is doping methane with hydrogen; this would allow a number of the benefits to be realised whilst allowing the current infrastructure to be utilised.

II. Background

This study has focussed on the low-swirl flame first noticed by Cheng, R.K., this is largely due to its inherent low NOx emissions, but also due to the change in structure caused by hydrogen addition.

The low swirl design differs significantly from the more common high swirl concept in that the latter utilises a recirculation region caused by strong vortices to ensure the flame is kept stable. Whereas the low swirl concept uses low swirl intensities that are too weak to generate the kind of vortex breakdown required to generate intense recirculation, instead it relies on flow divergence to ensure flame stability. The swirl structure must be achieved via the use of a low swirl injector or micro-jets. The key difference between the low swirl injector and a high swirl injector is the inner turbulence grid. This leads to two different zones within the flame - the outer swirling region which interacts with the surrounding air developing a shear layer, and the central zone. The latter of which does not exhibit the same complex flow features such as intense recirculation seen in high swirl flames. Figure 1 shows the structure of the low swirl injector modelled as part of this study.

Figure 1 - LSI c/w turbulence grid and swirl blades
Image from: [17]

Figure 2 - Detached low swirl flame
Image from: [22]

The detached flame can be seen in Figure 2, this shows how the flame is aerodynamically stabilised a distance from the burner outlet. The flame front occurs at the point at which the local fluid velocity equals the turbulent flame speed (U_t) leading to a stabilized detached flame. As the level of hydrogen doping increases the U_t also increases, this causes the flame front to move closer to the burner outlet.

III. Flame structure

In the study Numerical simulation of Lewis number effects on lean premixed flames by Bell, et al., [2], PLIF imagery of the flame front was used to identify the distribution of the radical OH. The results of this can be seen in Figure .

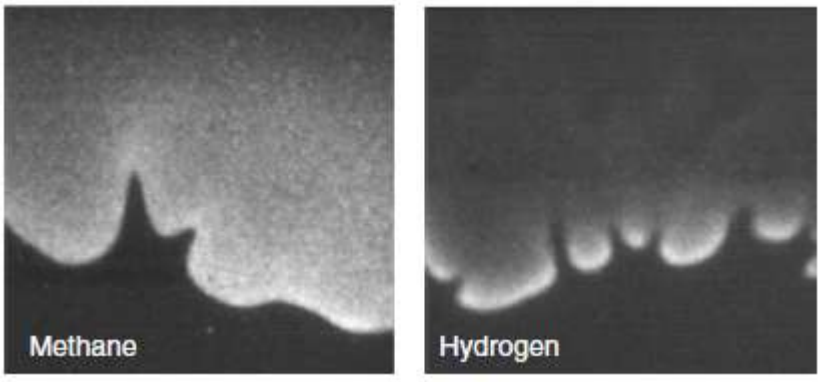

Figure 3 - PLIF images (OH profiles) of methane and hydrogen flames
Image from: [2]

These images show the differences between the two flames, firstly the hydrogen flame exhibits significantly more wrinkling due to the flames thermo-diffusively unstable nature. It can also be seen that the high OH concentrations are located at the peaks of the wrinkles in the hydrogen flame whereas they are located in the troughs in the methane flame. Finally, the OH distribution varies significantly in the hydrogen flame because the reaction takes place in 'cells' due to local extinction in the troughs versus the continuous reaction zone in the methane flame. This cellular structure is due to the highly diffusive nature of hydrogen causing Soret diffusion. Whilst hydrogen can tolerate a higher strain rate before extinction – 1061 s^{-1} versus 326 s^{-1} [3], should extinction occur the majority of the reactants in the region diffuse towards the strong reactions on either side. This is possible because the reactants diffuse out of the region quicker than they can be heated to ignition temperature by the surrounding reactions. These structures are reasonably stable and do

not typically re-ignite but, different cells can merge (see [2]). Two further changes are an increase in the turbulent flame speed and the flame area the latter of which results from the decrease in chemical time-scale, due to the flame being better able to respond to changes in strain.

IV. Existing works

To date the k-ε model has been one of the most commonly used models in industry, although when applied to low-swirl flames a modification has typically been employed. In the work of Eldrainy, et al., however, the standard model was utilised and reasonable agreement was found with experimental data [4]. In the works by Mameri, et al,. [5] the k-epsilon model with the correction developed by Pope in tandem with the EDM combustion model was found to show good agreement between numerical and experimental. Similar good correlation was also found in a study by Mardani, et al. [6]. A study completed by Saqr, et al. [7] found the standard k-ε model to be inferior when compared to the Rε/k – ε model. It was found that the Realizable model predicted the forced vortex flow particularly well [7] which form a crucial flow phenomena in a swirl stabilised flame. In a broader study Engdar and Klingmann assessed the performance of a number of two equation models when applied to a confined swirling flow [8]. The k-ε, Chen's k-ε, curvature modified k-ε, k-ω and SST- k-ω models were assessed at two swirl values – 0.33 and 0.58. The authors found that at the higher swirl value the spread of results from the different turbulence models increased significantly with the k-ε and curvature modified k-ε failing to predict the reversal of portions of the flow [8]. The best performing model at this swirl value was the SST K-ω, however this still over predicted the axial velocity values by a factor of two in places [8]. Specifically in regard to the low-swirl flame Muppala, et al. found good agreement with experimental data using the RNG k-ε model in tandem with a modified reaction model [9], whereas Rohani & Saqr utilised the realizable k-ε [10]. Rohani & Saqr based this decision on the work of Shih et al; who demonstrated that the Realizable k-ε model consistently outperformed the standard model across a wide variety of tests [11]. However, it was highlighted that to obtain the greatest accuracy this model should be used in tandem with a flamelet model [10]. For additional studies utilising the k-ε model please see [10].

The RSM family of turbulence models have been used extensively to simulate this type of flow, however very mixed results have been obtained. Su, et al. used the RSM model to simulate the suspension flow in a square cyclone and obtained aceptable results indicating that the model was suitable for this type of flow [12]. In addition to this Jawarneh & Vatista used the RSM model to model a strongly swirling chamber flow [13] and obtained excellent agreement with experimental data. However in the study Investigations in the TECFLAM swirling diffusion flame: Laser Raman measurements and CFD calculations, Meier, et al., found relatively poor agreement with experimental data. However, Meier, et al also stated that a number of alternative turbulence models and settings had been tried to no avail so this would appear to not be unique to this model family [14].

Cold data was not available for the main verification study so an alternative study had to be utilised. In this case this was taken from the study Fuel effects on a low-swirl injector for lean pre-mixed gas turbines by Littlejohn & Cheng. This study also utilised a low swirl injector, but at a lower fluid velocity and at a slightly higher vane angle – 42^0 vs 40^0 in the main study. It was this reports opinion that despite these minor modifications the findings from this study could still be applied to the reacting study. The validation data for the reacting section of this project was taken from the study Laboratory investigations of a low-swirl injector with H_2 and CH_4 at gas turbine conditions by Cheng, et al., [15]. In this study a series of experiments were conducted where the hydrogen composition was varied from 0-100% for a number of different inlet velocities and pressures. In order to assess the flame behaviour at possible industrial conditions the intial pressure was atmospheric, this was then increased up to approximately gas turbine conditions. The table below gives the experimental inlet conditions for the series of reacting cases based on the study conducted by Cheng, et al,. however has been taken from the works of Muppala, et al,. [9]

Table 1 - Experimental inflow conditions, U = 18 m/s and P = 1 bar

Equivalence ratio	H_2 vol %	$\rho_{Unburnt}$ kg/m^3	ρ_{Burnt} kg/m^3	$T_{adiabatic}$ K	$Le_{effective}$	U_{Lo} m/s	α x10^5 m^2/s	ν x10^5 m^2/s
0.59	0	1.1268	0.2095	1610	0.9550	0.1042	2.0000	1.6100
0.40	40	1.1140	0.2360	1416	0.4980	0.0694	2.1600	1.6500
0.40	60	1.0960	0.2215	1495	0.4019	0.1160	2.3000	1.6600
0.40	80	1.0650	0.2096	1557	0.3360	0.1933	2.5500	1.7100
0.40	100	1.0010	0.1975	1614	0.2900	0.3020	3.0500	1.8100

V. Modelling

The RANS approach to turbulence modelling has been discussed extensively in literature so this has not been discussed here, see [16] for further details. Reaction models describe the progress of the reaction using the reaction progress variable c, here the reactants are 'c=o' and the products are 'c=1'. The value of c therefore changes from 0 to 1 across the flame brush. The mean reaction progress variable is then used to model flame front propagation which is represented by $\bar{c}$, this is achieved via the solution of the equation below:

$$\frac{\partial}{\partial t}(\rho\bar{c}) + \nabla * (\rho\overline{vc}) = \nabla * \left(\frac{\mu_i}{Sc_i}\nabla\bar{c}\right) + \rho S_c$$

Equation 1 - Premixed reaction model

$$\rho S_c = \rho_u U_t |\nabla_c|$$

Equation 2 - Mean reaction rate

Zimont turbulent flame speed model

$$U_t = A(\acute{u})^{\frac{3}{4}} U_l^{\frac{1}{2}} \alpha^{\frac{-1}{4}} l_t^{\frac{1}{4}} \quad \text{or} \quad U_t = A\acute{u}\left(\frac{\tau_t}{\tau_{chem}}\right)^{\frac{1}{4}}$$

Equation 3 - Zimont turbulent flame speed model

[16]

Peters flame speed model

The Peters flame model relies on a greater number of empirically derived constants which gives it the appearance of a more complex model, this can be seen below:

$$U_t = U_l(1 + \sigma_t)$$

Equation 4 - Peters turbulent flame speed model (1)

$$\sigma_t = -\frac{a_4 b_3^2}{4b_1}\frac{l_f}{\delta}l_*^q + \left[\left(\frac{a_4 b_3^2}{4b_1}\frac{l_f}{\delta}l_*^q\right)^2 + \frac{C_s b_3^2}{2}\frac{\acute{u} l_f^2}{U_l \delta l_t}\right]^{\frac{1}{2}}$$

Equation 5 - Peters turbulent flame speed model (2)

[16]

VI. Numerical set up

The solid geometry used to generate the mesh can be seen below, this was modelled in Solidworks and then imported into ANSYS ICEM. It was developed in line with the dimensions given by Muppala, et al, [17] and Cheng, et al, [15], the solid geometry and the corresponding numerical grid can be seen in Fig. 4 and Fig. 5.

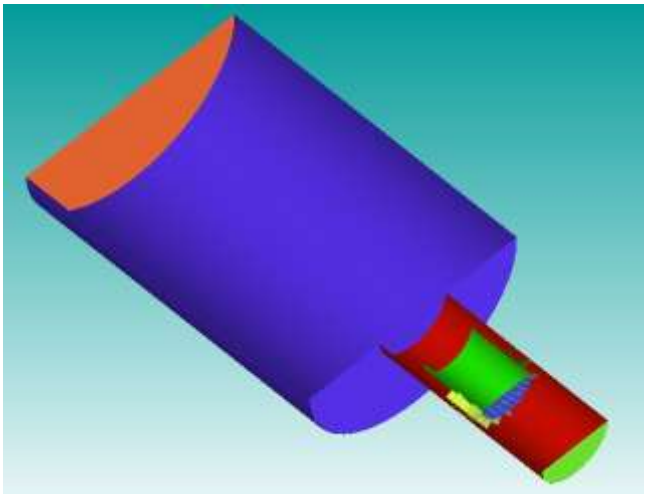

Figure 4- Cut out view of solid geometry

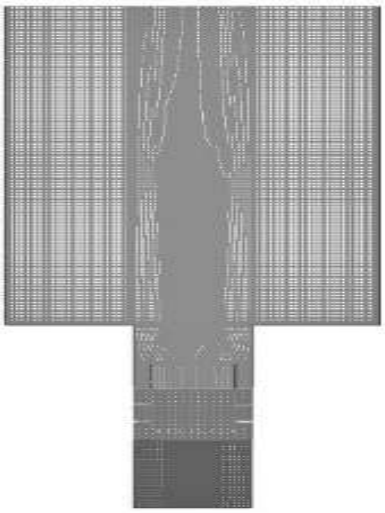

Figure 5 - Numerical geometry

The dimensions of the final numerical grid can be seen below:

Table 2 - Numerical grid dimensions

Entity	Value
Combustor far-field	2.0 mm
Combustor near wall	0.5mm
Shear layer	0.5mm
Core	0.9mm
LSI far-field	0.9mm
LSI near wall	0.6mm
Pre-swirl far-field	2mm
Pre-swirl near wall	0.5mm
Total no of elements	**3892722**

The table below gives the initial Fluent settings for the remainder of this study,

Table 3- Fluent settings

Setting	Value
Momentum scheme	1st order then re-run with 2nd order
Pressure scheme	PRESTO!
Pressure-Velocity coupling	SIMPLE
Turbulence dissipation scheme	1st order then re-run with 2nd order
Turbulence energy scheme	1st order then re-run with 2nd order
Reynolds stress scheme	1st order then re-run with 2nd order

VII. Turbulence Model Study

Due to the conflicting conclusions drawn from literature this study was conducted to establish the most effective turbulence model for the low-swirl flame. The four most successful turbulence models have been selected from literature and have been assessed for this flame. As previously discussed minor modifications were made to the geometry and flow conditions for this section of the study due to cold flow data being unavailable for the primary verification set. Please note each of the grids used for the different turbulence model were shown to be independent individually to ensure the reliability of the results. The validation stage has unfortunately not yielded the level of correlation intended, however, there are a number of key points that can still be drawn.

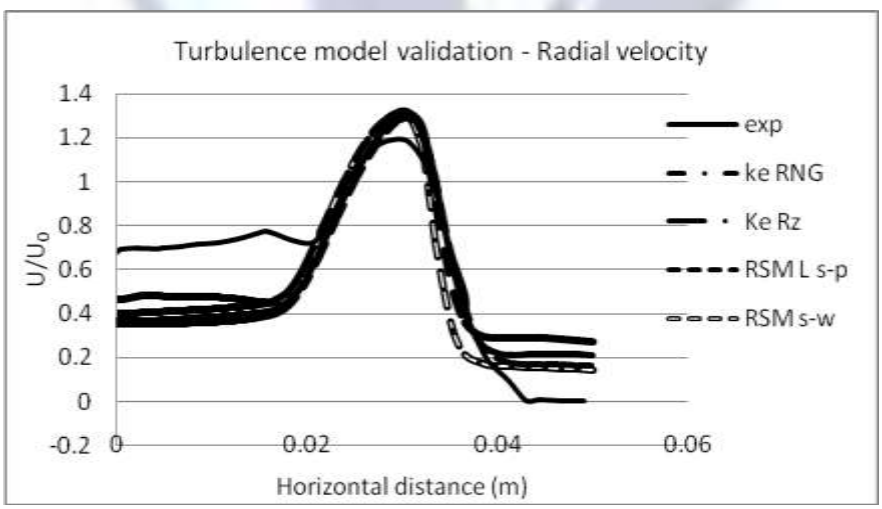

Figure 6 - Validation set - Experimental results obtained from Littlejohn & Cheng, 2007

Reasonable correlation can be seen in the location of the maximum velocity, however the maximum velocity itself was slightly over predicted (8% over prediction). The central region indicates that one of a number of approximations that had to be made regarding the geometry was incorrect, clearly the turbulence grid restricted the flow excessively resulting in the under prediction of velocities within this region. As a result of this and as all four turbulence models

showed reasonable correlation this was discounted as an issue. In terms of individual model performance both of the RSM models predicted asymmetrical velocities in the outer regions which was not in-line with the experimental results. The stress-omega model also showed a steeper decline in velocity as compared to the experimental results. The k-ε RNG model significantly over predicted the velocities in the outer regions and was therefore deemed unacceptable for this study. This left the k-ε Rz model which converged approximately 800 iterations before the RSM Linear Stress-Pressure model (the next best performing model), this clearly made this model the optimal choice for this study.

VIII. Methane/Air Results

As a precursor to the enriched studies a pure methane study was completed in order to provide a measure of the different combustion models performance when applied to traditional fuels. As the reaction models were initially proposed with this type of hydrocarbon in mind it was expected that a good degree of correlation would be found between the experimental results and the numerical results. To this end a modification to the Zimont model turbulent flame speed constant proposed by ANSYS was trialled and the performance of the different ECFM closure options assessed.

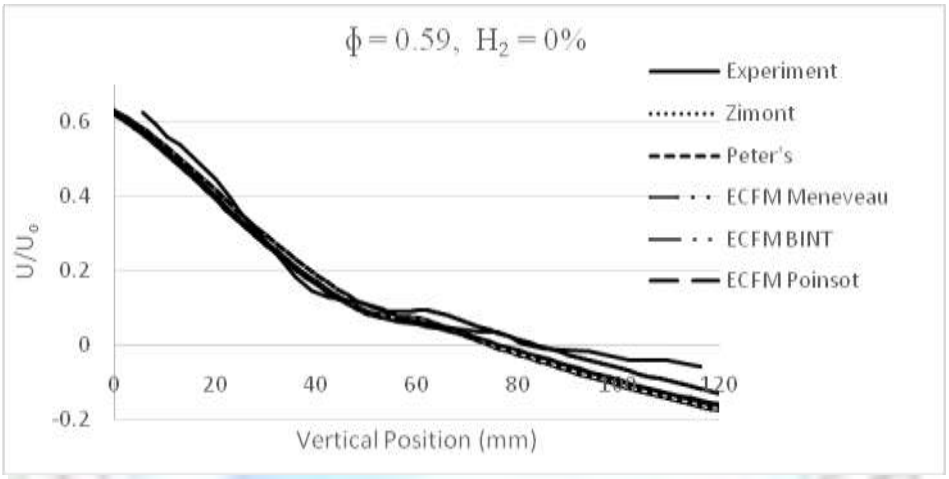

Figure 7 - Axial profile of axial velocity for 100% methane, Zimont and Peter's turbulent flame speed models are compared with experimental data and the ECFM model with three closure options. ϕ=0.59, U_o=18 m/s

The unmodified Zimont model and the Peter's model show reasonably good correlation with the experimental data, however the flame front has been predicted to lie slightly further from the combustor inlet. The experimental data shows the flame front occurs at approximately 41mm from the inlet whereas the numerical results predict that the flame front would develop at approximately 50mm from the inlet. This inaccuracy appears to be relatively constant across all of the trialled models. Beyond 100mm the results clearly begin to diverge from the experimental trend. This has tentatively been attributed to an over prediction in the axial velocity on the part of the RANS model, which was also seen in the work of Meier, et al [14]. The ECFM Poinsot model shows reasonable agreement with the validation set and a marginal improvement over the Bint and Meneveau closure options. However, if Fig. 7 is consulted this agreement is called into question.

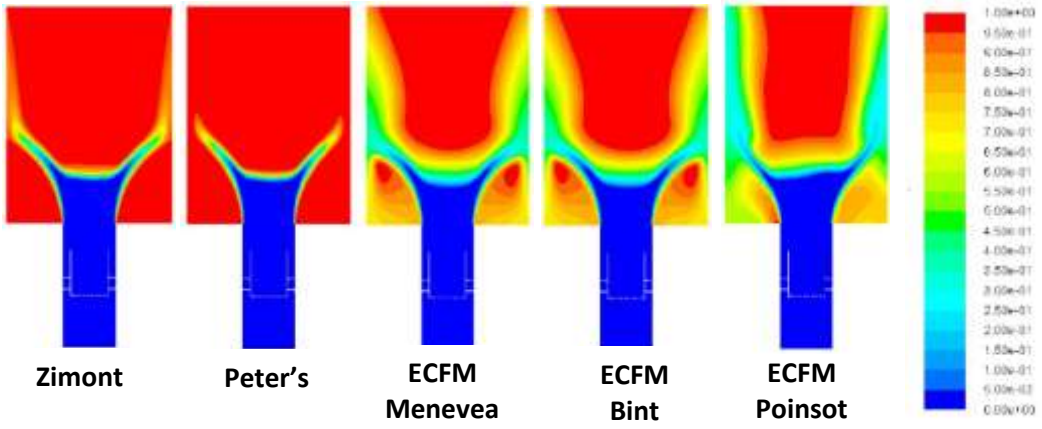

Figure 8 - Mean reaction progress variable for 100% methane ϕ=0.59, U_o=18 m/s

Figure

Fig. 8 shows the mean reaction progress variable for the different models, the Peter's and Zimont models have predicted a localised flame, stabilised just above the inlet to the combustor, which was in-line with expectations. However, the ECFM model has predicted a far more diffusive flame with flame pockets existing in the corners and up the sides of the combustor. Once again the Meneveau and Bint closed models have produced very similar results with the Poinsot closed ECFM model.

IX. Enriched Results

The following results show the numerical predictions for four different levels of hydrogen enrichment – 40, 60, 80 and 100% for the unmodified Zimont, Peters and ECFM (Poinsot) models. All flow conditions, aside from the equivalence ratio which was changed to 0.4, were as per the methane study. Examining the progress variable contour plots in Figure it can be seen that the ECFM model predicts reaction to occur on the wall of the combustor which is not in-line with experimental observations. However, the flame shows significant change with the addition of hydrogen showing that the model has predicted the increased reaction rate well. This indicates that the model may respond positively to tuning, however there was not sufficient time to explore this possibility. The performance of this model was partly in contrast to expectations as the additional variable flame surface density gives the flame surface area per unit volume and should allow a more detailed prediction of the flame intensity and location. The former would appear to have been well accounted for, but the flame location was not in line with the experimental findings, and the simpler 'C' equation models appear to have performed better in this regard.

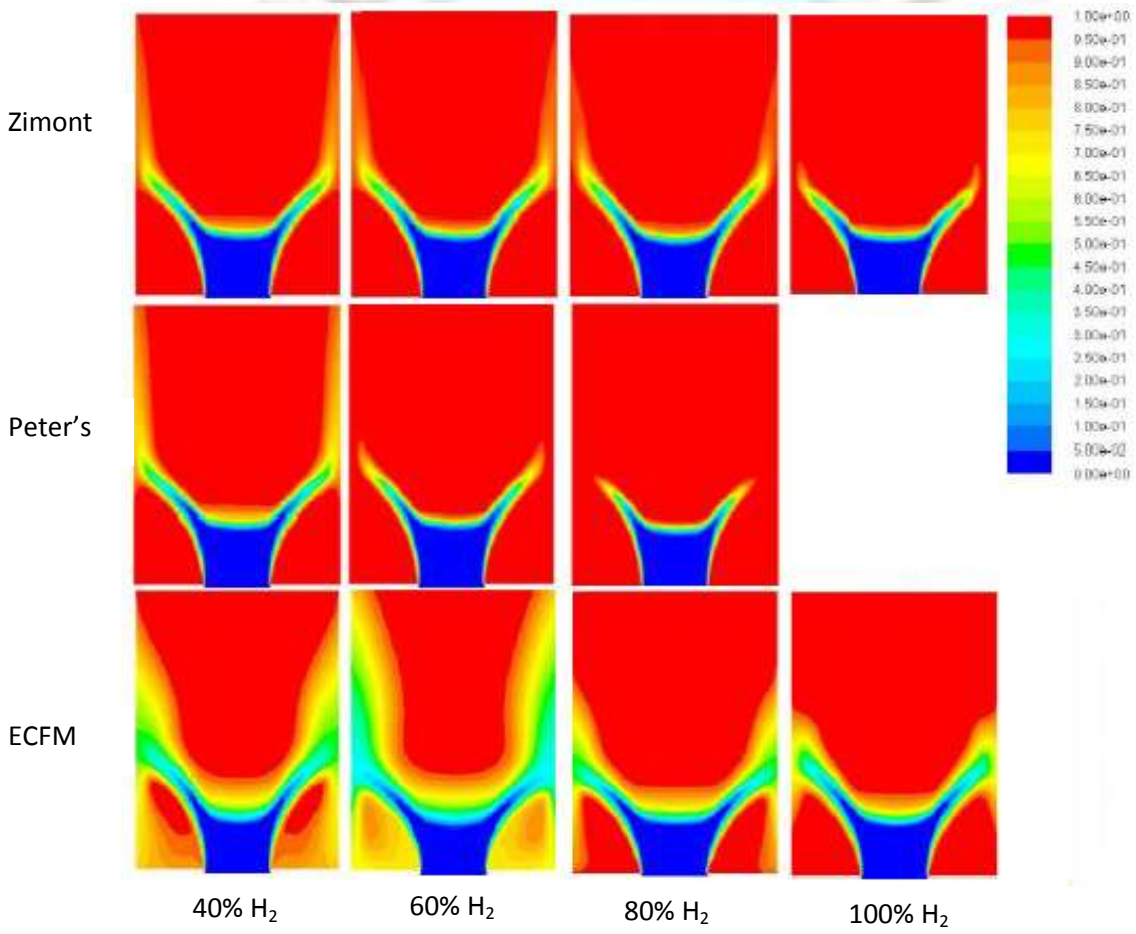

Figure 9 - Mean reaction progress variable for hydrogen enrichment levels 40-100%, Zimont, Peters and ERSM Poinsot models. ϕ=0.4, Uo=18 m/s

The Peter's model has also predicted the increased reaction rate with the size of the flame decreasing significantly with hydrogen addition. Unfortunately, the Peter's model predicted that the flame would flash back at 100% hydrogen which was not in line with experimental findings. It is likely that the model was over-compensating for the increased reactivity of hydrogen. The Zimont model did not show such a significant change in flame size with hydrogen addition as the other two models, but provided predictions across the full range of enrichment. None of the models have

predicted the shift in the flame front towards the inlet and consequently the flame is not anchored to the inlet at 100% hydrogen in any of the models. Whilst each model has, to some extent, accounted for the increase in burning intensity resulting in reduction in flame size (constant flame shape) clearly not all of the behaviour has been captured.

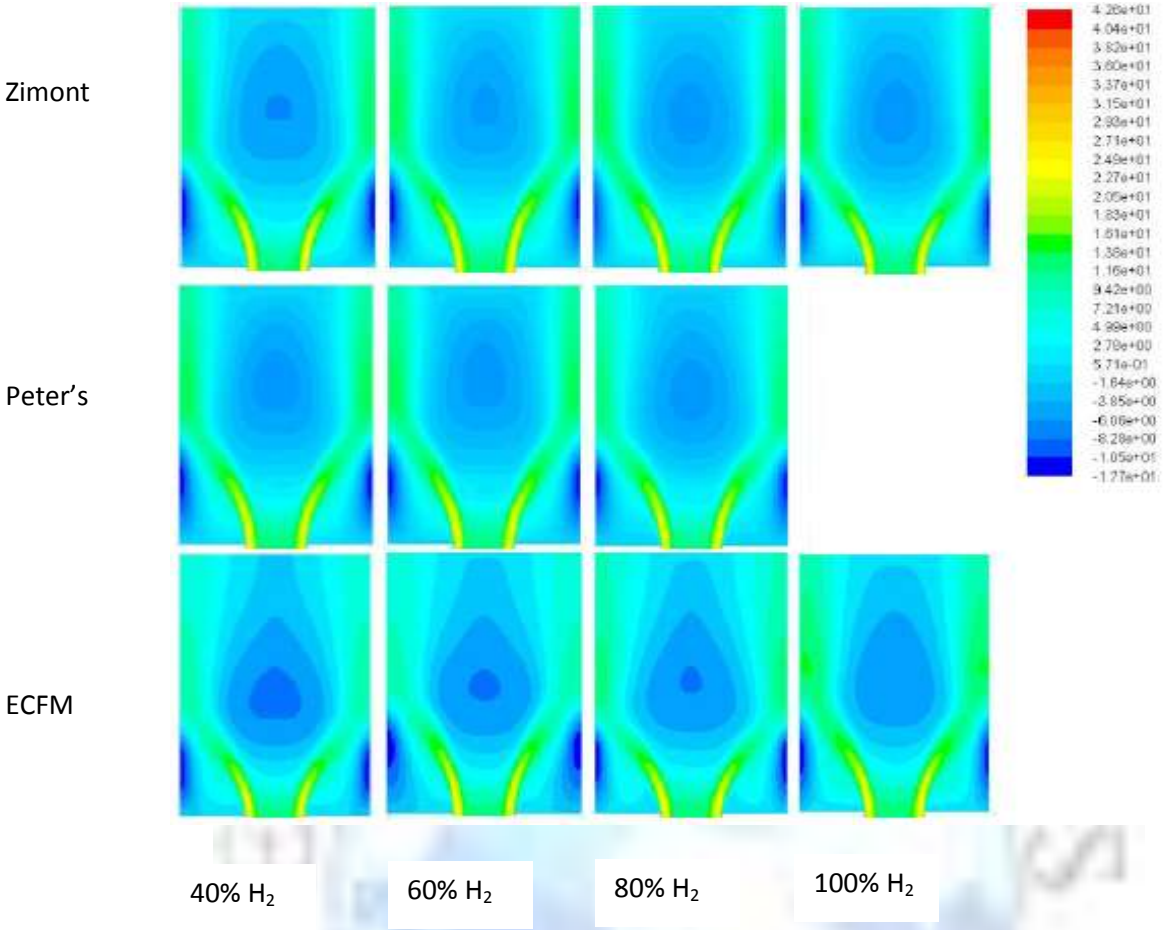

Figure 10 - Mean axial velocity for hydrogen enrichment levels 40-100%, Zimont, Peters and ERSM Poinsot models. ϕ=0.4, Uo=18 m/s

Fig. 10 shows that significant change occurs in ECFM predictions of both the shape and size of the recirculation region with hydrogen enrichment. The fluid velocity can also be seen to increase in the reaction zone indicating the model produces a reasonable non-physical representation of the increased reaction rate caused by the increased concentration of the OH radical observed by Schefer, [18]. The increased robustness of the flame, as discussed previously, would also play a role here. This was included in the analysis using an approximate critical strain rate for each mixture. The Zimont and Peters models show some change in the recirculation magnitude, but this was not as pronounced as with the ECFM model. The increase in velocity in the reacting region is also not as clear.

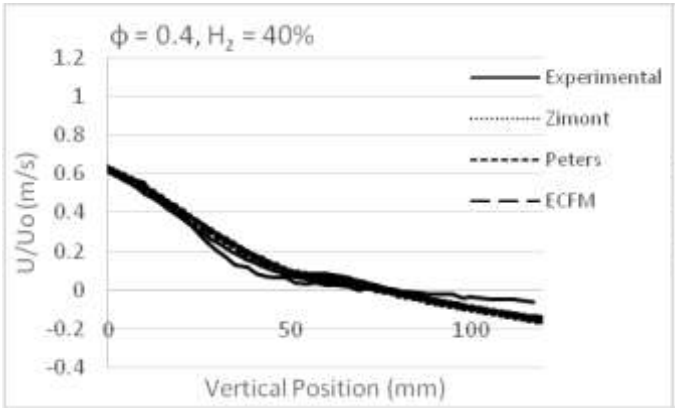

Figure 11 - Axial profile of axial velocity for 40% hydrogen, Zimont and Peter's turbulent flame speed models are compared with experimental data and the ECFM model. ϕ=0.4, Uo=18 m/s

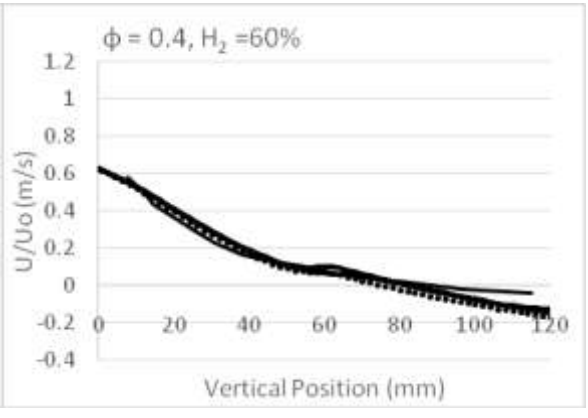

Figure 12 - Axial profile of axial velocity for 60% hydrogen, Zimont and Peter's turbulent flame speed models are compared with experimental data and the ECFM model. ϕ=0.4, Uo=18 m/s

Figure 11 shows the axial profile of axial velocity for 40% hydrogen: once again the results can be seen to diverge further away from the inlet of the combustor, in this case around 70mm. This, as previously discussed, has been attributed to an over-prediction of axial velocity on the part of the RANS model. The predicted flame front location was approximately 10mm further downstream as compared to the experimental data seen in the methane study.

Very similar results can be seen in the 60% plot (Figure 12). Again the flame front was predicted to lie further upstream as compared to the experimental data and beyond 70mm the results can be seen to diverge from the experimental trend. The Peters model has predicted a slight increase in axial velocity at the location of the flame front at 60% enrichment, but it can be more clearly seen at 80% enrichment. In the experimental set this was caused by the raised concentration of OH radicals causing a surge in the reaction rate. The effect of this can be seen more clearly at 80% enrichment and above.

The accuracy of the numerical predictions at 80% hydrogen (Fig. 13) and above deteriorates significantly to essentially

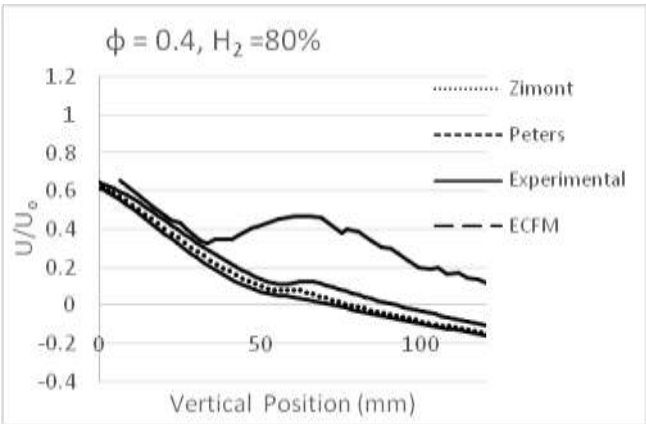

Figure 13- Axial profile of axial velocity for 80% hydrogen, Zimont and Peter's turbulent flame speed models are compared with experimental data and the ECFM model. ϕ=0.4, Uo=18 m/s

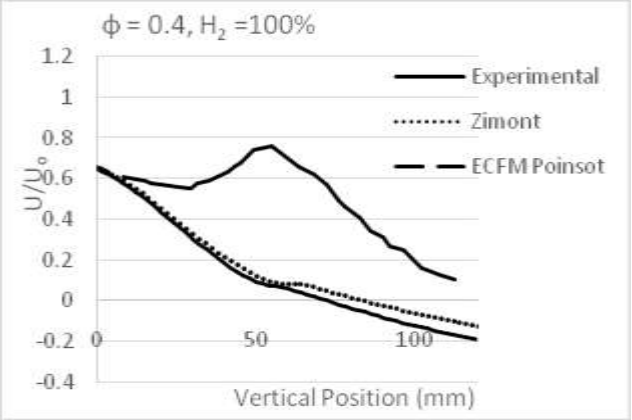

Figure 14- Axial profile of axial velocity for 100% hydrogen, Zimont and Peter's turbulent flame speed models are compared with experimental data and the ECFM model. ϕ=0.4, Uo=18 m/s

no correlation at 100% hydrogen (Fig. 14). The Zimont model predicts a very slight increase in velocity at the flame front for 100% hydrogen, but it falls well short of the experimental data. Also none of the models predict the movement upstream of the flame front, which can clearly be seen in the experimental data. This means that the models, whilst being capable of producing a non-physical estimation of the behaviour resulting from the increase in OH radicals, provided a relatively poor output.

X. Model Modification

The standard form of the Zimont model can be seen below with the turbulent flame speed constant highlighted in bold.

$$U_t = \boldsymbol{A}(\acute{u})^{\frac{3}{4}} U_l^{\frac{1}{2}} \alpha^{\frac{-1}{4}} l_t^{\frac{1}{4}}$$

Equation 6- Zimont turbulent flame speed model [16]

This was the term that was initially modified in an effort to improve the performance of the Zimont model as applied to this case. This was achieved via an iterative process, but by consulting the turbulent flame speed plots produced by the initial simulation runs a sensible starting point was established. As the experimental flame front location was approximately 15mm from the inlet to the combustor, at which point the fluid velocity was approximately 9m/s, the turbulent flame speed would need to increase by a factor of approximately 4.5 to exist at this location.

This gave a starting constant of 2.34. It should be highlighted at this stage that this analysis was significantly over simplified as the terms within the reaction model do not all behave in a linear fashion and there is a significant amount of interaction between the various terms. This then means the location of the flame front and the turbulent flame speed at that location will affect the fluid velocity and vice versa, but as a starting point this was deemed an adequate level of accuracy. The final value for 80 and 100% hydrogen can be seen below along with the results. As reasonable agreement could be seen below 80% enrichment there was no need to attempt to tune the model.

Table 4 - Final tuning values for each mixture

Mixture	Constant value
80% Hydrogen	0.741
100% Hydrogen	1.85

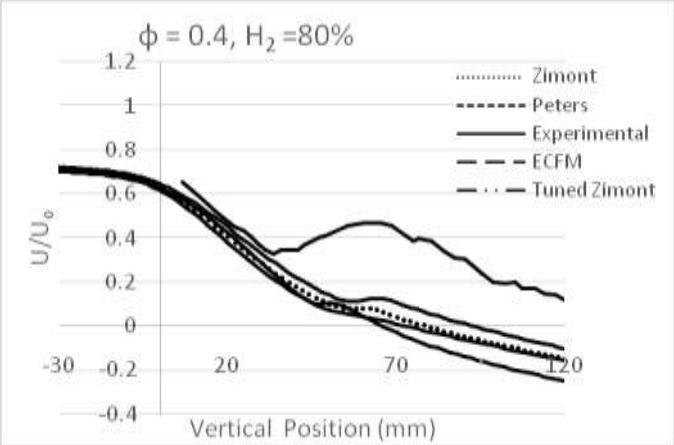

Figure 15- Axial profile of axial velocity for 80% hydrogen, Standard Zimont and tuned Zimont turbulent flame speed models are compared with experimental data and the ECFM model. ϕ=0.4, Uo=18 m/s

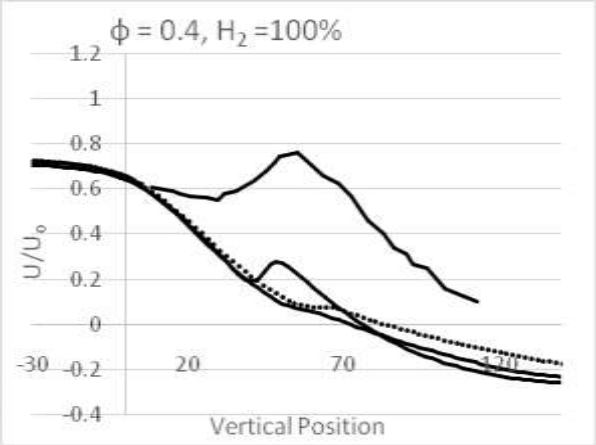

Figure 16 - Axial profile of axial velocity for 100% hydrogen, Standard Zimont and tuned Zimont turbulent flame speed models are compared with experimental data and the ECFM model. ϕ=0.4, Uo=18 m/s

If the figures above are consulted it can be seen whilst some improvement in the results had been achieved the agreement with experimental data was still relatively poor. This was largely because of the transitory behaviour of the turbulent flame speed in the preliminary sections of the combustor causing the flame to flash back. As reaction models are relatively simple models the key method of predicting flame stabilisation derives from the turbulent flame speed. As a result of this an increase in the turbulent flame speed beyond the local fluid velocity at any point in the preliminary section results in a prediction of flashback.

As a result of the limited improvement seen from modifying the turbulent flame speed constant this study has developed a modification in the form of four additional terms. However, before stating them, a brief discussion of the intended formulation has been provided There are two core hypothesis published by Damköhler within which he identified two different flame regimes which he termed large scale and small scale turbulence, which correlate to the corrugated/wrinkled and thin reactions zones respectively on the Borghi diagram [19]. Damköhler then made two statements:

- In the large scale regime turbulent flame speed scales with turbulence intensity
- In the small scale regime turbulent flame speed scales with the square root of turbulent diffusivity divided by the chemical time scale.

[20]

Please note turbulent intensity may be approximated from:

$$I \equiv \frac{u'}{U_{avg}}$$

Equation 7 - Turbulent Intensity

[21]

As hydrogen flames largely exist in the flamelet regime and can be located in the corresponding region on the Borghi diagram, it therefore follows that the modification should be a function of the RMS velocity fluctuations. If it could also include a consideration towards the small scale region the modification would likely be more robust as with a significant increase in turbulence the flame could feasibly shift regime, however unlikely this maybe. Hence the following statement can be made:

$$\text{Modification} \equiv f\left(u', \frac{1}{\tau_{chem}}, \text{an appropriate addition turbulent quantity}\right)$$

A number of different combinations of terms were trialled all of which were developed based on the above stipulation, the best performing of these can be stated as:

$$\frac{\mu_T}{k\tau_{chem}}$$

Expression 1 - Modification proposed by this project

This can then be simplified to

$$\grave{A} \cdot \frac{U_l}{u'} \cdot \frac{l}{l_f} \approx \grave{A} \cdot Da$$

Equation 8 - Simplified form of proposed modification

These two fractions can then be recognised as the inverse of the vertical axis component of the Borghi diagram and the latter the horizontal axis component of the Borghi diagram. The function can then be further simplified using the definition for the Damkohler number. The modified form can then be stated as:

$$U_t = \text{Absolute}\left(\frac{A}{\exp^{Le\,Eff-1}} (\acute{u})^{\frac{3}{4}} U_l^{\frac{1}{2}} \alpha^{\frac{-1}{4}} l_t^{\frac{1}{4}} \frac{\mu_T}{k\tau_{chem}}\right)$$

Equation 9 - Modified Zimont turbulent flame speed model

The effective Lewis number term has been taken from literature [9] and contributes towards accounting for the varying diffusivity of the hydrogen/methane mixtures. This means that this element focusses particularly on the 80% hydrogen case with limited scope at 100% hydrogen.

RESULTS

The results produced by the modified Zimont model can be seen below:

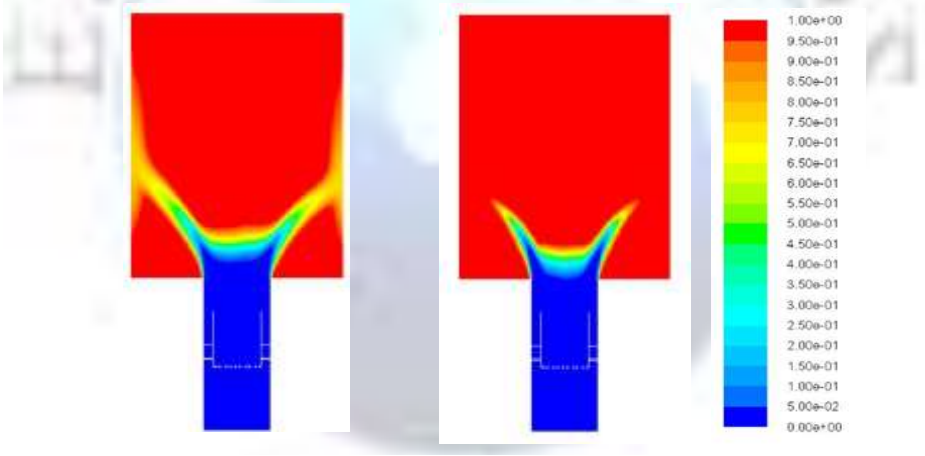

Figure 17 - Mean reaction progress variable contour plots - Left 80% hydrogen, Right 100% hydrogen, Modified Zimont model

The contour plots shown in Fig 17 show the reduction in the flame size indicating that the increased reaction intensity has been correctly predicted. The modified model has also predicted the shift of the flame front and the core reaction zone has deepened indicating that the burning in the shear layer has also been predicted. This has been confirmed by examining the axial velocity later in this section. However, it should be highlighted that a change in flame shape was observed in the experimental study which has not been predicted by the numerical study.

A significant reduction in the reacting plumes shows the shift away from the 'M' shaped flame has been partially predicted, but the planar structure seen in Figure differs significantly. However it should be highlighted that the experimental observations were based on visible luminosity and it is known that hydrogen flames exhibit considerably reduced visible emissions. Depending on the light conditions, which are not known for the experimental findings, these emissions are so weak that portions of the flame would not be visible to the human eye. It should also be noted that the emissions that can be observed are largely due to hydrocarbon impurities in the hydrogen so if high purity hydrogen was employed in this study the emissions would have been reduced further.

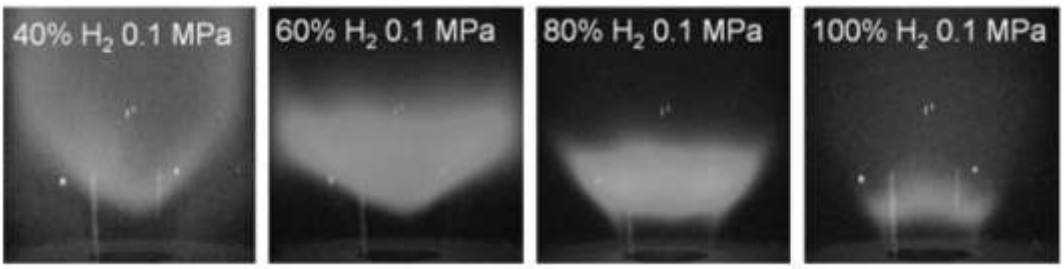

Figure 18 - Visible luminosity of methane/hydrogen flames, 0.1MPa. ϕ=0.4, Uo=18 m/s
Image from: [15]

Hence, whilst this report has highlighted a possible disagreement with the experimental observations this would warrant further experimental investigations to ensure the two data sets are actually comparable. The physical basis behind this change in shape can be seen to be due to burning in the outer recirculation region (shear layer). This can be seen in the modified Zimont model progress variable plots as the unburnt fuel section of the plumes has decreased significantly whereas the unmodified model has not predicted this feature. The increase in burning in the outer shear layer can also be seen in Fig. 18.

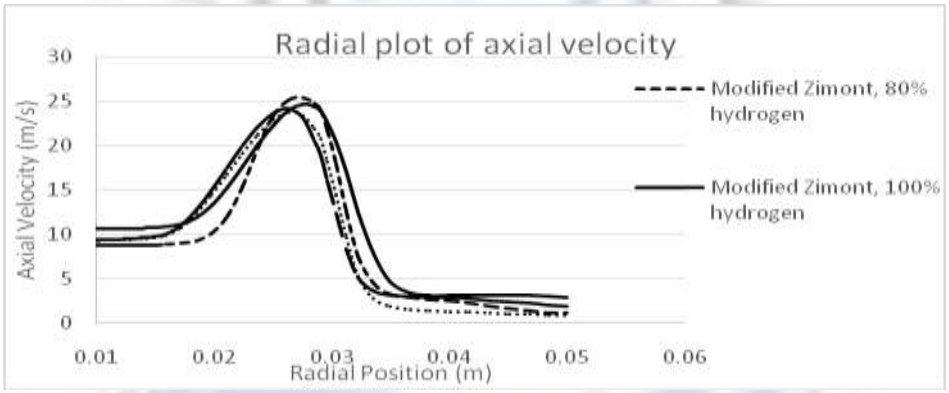

Figure 19 - Radial plot of axial velocity, y = 15mm from combustor inlet. Comparison of unmodified and modified Zimont models. ϕ=0.4, Uo=18 m/s

Fig. 19 compares the axial velocity predictions produced by the modified and unmodified Zimont models. The modified model has predicted the expansion of the shear regions between 80% and 100% hydrogen due to increased burning in the outer recirculation region, which is represented on the plot as a wider region of increased axial velocity. This further corroborates the modified models ability to predict the burning in the outer shear layer whereas the unmodified model shows no expansion between the two enrichment levels. This indicates that the burning in the outer recirculation region has not been predicted.

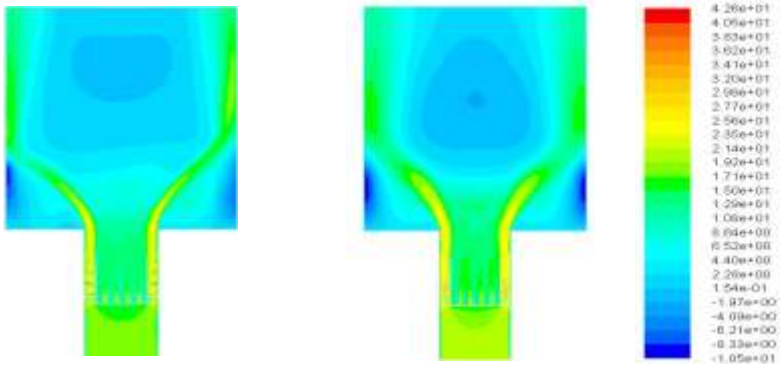

Figure 20 - Axial velocity contour plots - Left 80% hydrogen, Right 100% hydrogen, Modified Zimont model

The axial velocity plots shown in Figure 20 show the increased axial velocity and the reduction in the size and magnitude of the recirculation region which is in-line with the experimental observations. As previously discussed this change in the recirculation region was due to a combination of the increased axial velocity and heat release rate, indicative of hydrogen combustion. Interestingly the 80% plot appears to not have quite stabilised with reduced fluid velocities at the inlet to the combustor. This possibly indicates that some further work is required to tune the modified model for the different mixtures. It could also be indicative of the experimentally observed flame instabilities attributed to intermittent burning in the outer shear layer [15]. It is questionable whether such a simple model would be able to capture this behaviour, determining this would require further investigation.

If the data shown in Figure 19 and Figure 20 is examined it can be seen that the modification has functioned rather well, predicting the shift in the flame front in both cases. The location of the 80% flame front has been predicted to lie slightly further towards the combustor inlet than seen in the experimental findings. This adds to the previous observation that further work is required to refine the performance of the model when applied to a mixture. It should be noted, however, that the peak axial velocity has been well predicted albeit shifted towards the combustor. It is this studies' opinion that the approximation of chemical time may be partly responsible for this. Studies in literature have found more success using the inverse of the experimentally observed critical strain rate. If an accurate set of critical strain rates were available then the implementation of these values should provide more accurate results.

The pure hydrogen plot given in Figure 21 shows that the location of the pure hydrogen flame front has been correctly predicted with a slight under prediction in the peak axial velocity in the reaction region. It is this report's opinion that given more time the model could be tuned to output the correct peak axial velocity, however due to the time and computational expense required this would have to form part of the suggested further work. This additional tuning should also go some way to address the discrepancy between the experimentally measured swirling fluid volume and the predicted volume as previously discussed.

One further comparison between the modified and the standard Zimont models has been included to illustrate the magnitude of the change in the predicted reaction rate between the two models. Figure 21 shows the product formation rate (proportional to the reaction rate) for both the modified and unmodified models at 80% and 100% hydrogen. In both cases an increase in formation rate has been predicted however the magnitude of the change and the final values are vastly different. The unmodified model has predicted a small increase in the product formation rate, likely due to the increased laminar flame speed of hydrogen, whereas the modified model has predicted a significantly larger increase. This shows that the laminar flame speed term has limited influence over the behaviour of the enriched flame with other factors playing a more significant role.

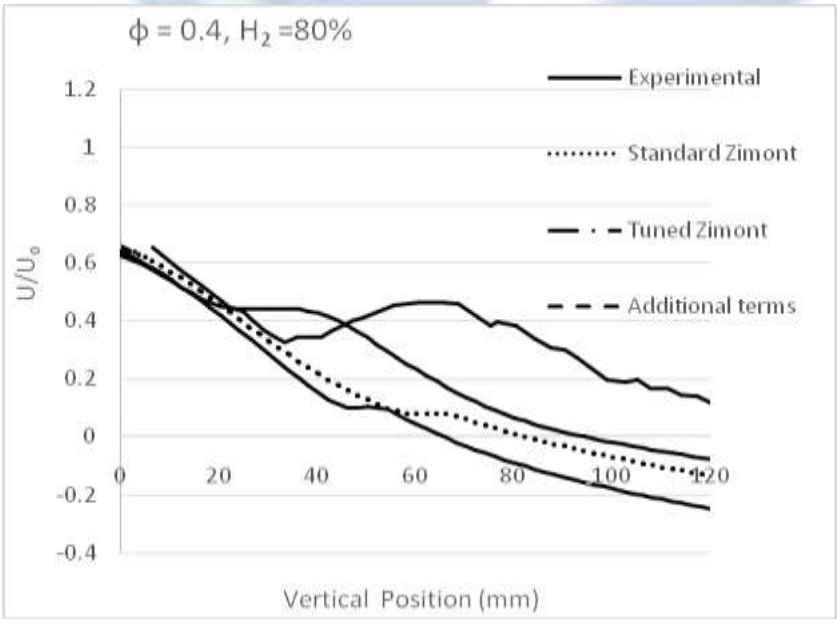

Figure 21 - Axial profile of axial velocity for 80% hydrogen, Standard Zimont, tuned Zimont and modified Zimont turbulent flame speed models are compared with experimental data. ϕ=0.4, Uo=18 m/s

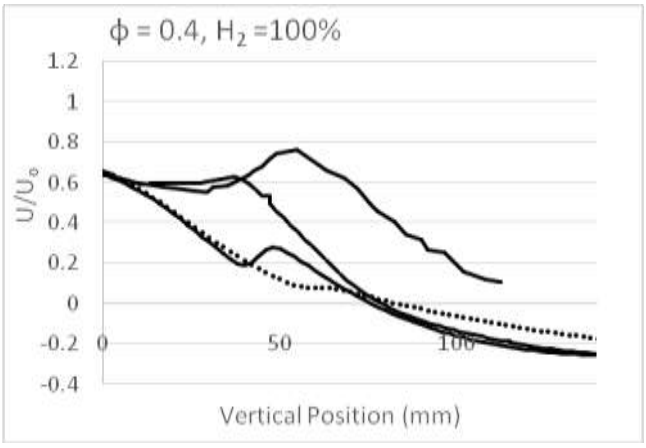

Figure 22 - Axial profile of axial velocity for 100% hydrogen, Standard Zimont, tuned Zimont and modified Zimont turbulent flame speed models are compared with experimental data. ϕ=0.4, Uo=18 m/s

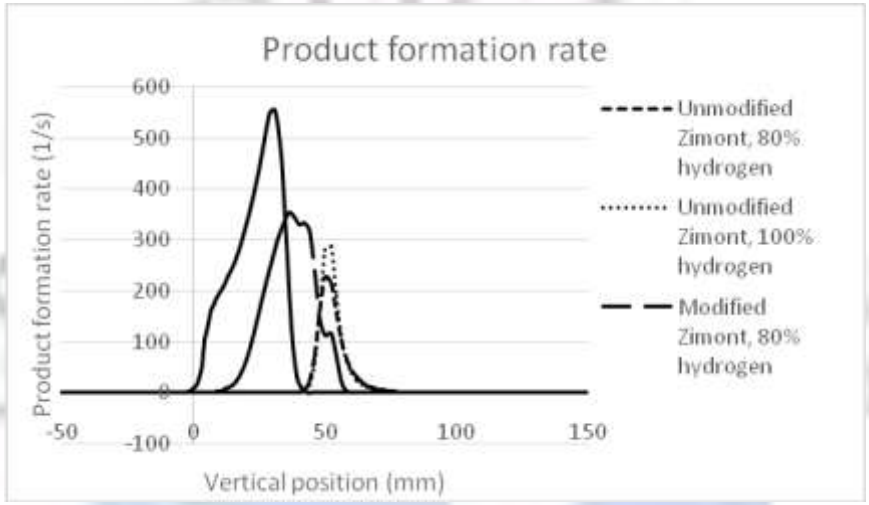

Figure 23 - Axial profile of product formation rate for 80% and 100% hydrogen. The standard Zimont model has been compared to the modified Zimont turbulent flame speed model. ϕ=0.4, Uo=18 m/s

One of these controlling/influential factors is the diffusivity of the fuel which has been accounted for with the inclusion of the effective Lewis number term taken from literature. However, this does not entirely account for the considerable difference seen in Fig 23.

It is the opinion of this report that this is due to the burning in the outer shear layer not being predicted by the unmodified model. This is considered to be one of the most obvious failings on the part of the unmodified model as experimental observations showed that the reactions in the shear layer facilitated the flames movement and eventual attachment to the combustor inlet. These reactions also increase heat release rate which in turn affects the recirculation region, one of the key turbulent features of the flame. This report further postulates that the increased heat rate and flame temperature would also cause an increase in the turbulent activity. This would indicate that the key consideration within the modification was that of the dependence of the turbulent flame speed on the RMS velocity (Damköhler's large scale hypothesis), which has previously been shown to be proportional to the turbulent intensity. The reaction induced turbulence would also cause an increase in the local turbulent kinetic energy, further indicating that the additional consideration of the turbulent quantities, which form the modification, are likely to have caused the improved results.

XI. Conclusion

To conclude, initially this study conducted a detailed literature search to identify any lessons that could be applied to this project. Whilst a number of parallels could be drawn from literature the conflicting findings led this report to conduct a solver settings and turbulence model study to establish the optimum set up for this project. This study then identified that no cold validation data was available for the main numerical geometry so an alternative was identified

and implemented in order to confirm that the correct cold flow physics were being captured. Due to a lack of information on the additional numerical geometry the correct dimensions of the turbulence grid could not be found which meant that only agreement in the reaction zone could be achieved. After obtaining reasonable agreement between the numerical predictions and the cold validation set within the key reaction zone this project conducted a number of reacting simulations. The findings from these have been summarised below:

- The Zimont model produced predictions at each level of enrichment and the results indicated that the increased reaction intensity resulting from the hydrogen addition had been partially accounted for in the numerical predictions. However, the shift in the flame front and the local increase in axial velocity in the reaction region were not adequately predicted.
- The Peter's model appeared to account for the increased reaction rate more effectively than the Zimont model, but it incorrectly predicted the flame would flash back at 100% hydrogen.
- The ECFM model accounted for the increase in reaction intensity well, but the initial predictions were so poor that good agreement was not found in any of the studies. The predictions of reactions occurring at the combustor wall were particularly erroneous.

As a result of these findings it can be said that the existing turbulent flame speed models functioned relatively well up to 60% hydrogen, but beyond this hydrogen plays the dominant role in the reaction and the accuracy degrades significantly. As a result it can be said that two regimes exist when considering the combustion of hydrogen/methane mixtures. In the first the reactivity of methane plays the dominant role due to the level of enrichment being inadequate for hydrogen to dramatically affect the process. Within the second the process is defined by the increased reactivity of hydrogen dramatically changing the behaviour of the flame. This change in behaviour is caused by the increase in the concentration of the OH radical which leads to burning in the shear layer which significantly changes the shape, structure and location of the flame front. The experimental data shows that this change begins when the hydrogen content increases beyond 60% and becomes particularly apparent at 80% and beyond.

Due to the poor agreement seen beyond 60% enrichment this project then set out to modify the best performing turbulent flame speed model, the Zimont model. This was carried out using a two pronged approach. Initially the turbulent flame speed constant was tuned, then a modification containing additional terms was developed and used in tandem with the exponential Lewis number term taken from literature [17]. The initial tuning of the turbulent flame speed constant did not produce a significant improvement in the level of agreement with the validation set, hence the additional terms were developed and implemented. The proposed modification has been shown to improve the accuracy of the results significantly particularly at 100% hydrogen with the location of the flame front being correctly predicted. However, the peak local velocity in the reaction zone was slightly under predicted, showing that there is still scope for further improvement. The level of agreement with the validation set deteriorated slightly for the mixed fuel (80% hydrogen) with the flame front being predicted to lie further towards the combustor than experimentally observed. It can however be said that the modification has improved the results significantly with the relationship between turbulent flame speed and RMS turbulent velocity highlighted as being they key element of this.

References

[1]. W. R. Bender, "Gas Turbine Handbook," 2006. [Online]. Available: http://www.netl.doe.gov/technologies/ coalpower/ Turbines /refshelf/handbook/TableofContents.html. [Accessed 24 12 2013].
[2]. J. B. Bell, R. K. Cheng, M. S. Day and I. G. Shepherd, "Numerical simulation of Lewis number effects on lean premixed flames," Proceedings of the Combustion Institute , vol. 31, pp. 1309-1317, 2007.
[3]. E. R. Hawkes and J. H. Chen, "Direct numerical simulation of hydrogen-enriched lean premixed methane-air flames," Combustion and Flame, vol. 138, pp. 242-258, 2004.
[4]. Y. A. Eldrainy, K. M. Saqr, H. S. Aly and M. N. M. Jaafar, "CFD insight of the flow dynamics in a novel swirler for gas turbine combustors," International Communications in Heat and Mass Transfer, vol. 36, pp. 936-941, 2009.
[5]. A. Mameri and I. Gokalp, "Numerical Simulation of Turbulent Methane Premixed Flames Enriched by Hydrogen," 2007.
[6]. A. Mardani, S. Tabejamaat and S. Hassanpour, "Numerical study of CO and CO2 formation in CH4/H2 blended flame under MILD conditions," Combustion and flame , vol. 160, pp. 1636-1649, 2013.
[7]. K. M. Saqr, H. I. Kassem, H. S. Aly and M. A. Wahid, "Computational study of decaying annular vortex flow using the Re/k-e turbulence model," Applied Mathematical Modelling, vol. 36, pp. 4652-4664, 2012.
[8]. U. Engdar and J. Klingmann, "Investigation of two-equation turbulence models applied to a confined axis-symmetric swirling flow," Computational technologies for Fluid/Thermal/Structural/Chemical systems with industrial applications, vol. 448, no. 2, pp. 199-206, 2002.
[9]. S. Muppala, B. Manickam and F. Dinkelacke, "A Comparative Study of Different Reaction Models for Turbulent Methane/Hydrogen/Air Combustion," READY FOR SUBMISSION.
[10]. B. Rohani and K. M. Saqr, "Effects of hydrogen addition on the structure and pollutant emissions of a turbulent unconfined swirling flame," International Communications in Heat and Mass Transfer, vol. 39, pp. 681-688, 2012.
[11]. T. Shih, W. Liou, A. Shabbir, Z. Yang and J. Zhu, "A New k-e Eddy Viscosity Model for High Reynolds Number Turbulent Flows-Model Development and Validation," NASA, Cleveland, 1994.

[12]. Y. Su, A. Zheng and B. Zhao, "Numerical simulation of effect of inlet configuration on square cyclone separator performance," Powder Technology , vol. 210, pp. 293-303, 2011.
[13]. A. M. Jawarneh and G. H. Vatistas, "Reynolds Stress Model in the Prediction of Confined Turbulent Swirling Flows," Journal of Fluids Engineering, vol. 128, pp. 1377-1382, 2006.
[14]. W. Meier, O. Keck, B. Noll, O. Kunz and W. Stricker, "Investigations in the TECFLAM swirling diffusion flame: Laser Raman Measurements and CFD Calculations," Applied Physics B, Lasers and Optics , vol. 71, pp. 725-731, 2000.
[15]. R. Cheng, D. Littlejohn, P. Strakey and T. Sidwell, "Laboratory investigations of a low-swirl injector with H2 and CH4 at gas turbine conditions," Proceedings of the Combustion Institute, vol. 21, no. 1, pp. 3001-3009, 2009.
[16]. Ansys Inc, Fluent Theory Guide, 14.5 ed., Canonsburg, 2012.
[17]. S. Muppala, B. Manickam and F. Dinkelacke, "A Comparative Study of Different Reaction Models for Turbulent Methane/Hydrogen/Air Combustion," READY FOR SUBMISSION.
[18]. R. W. Schefer, "Proceedings of the 2001 DOE hydrogen review: Combustion of hydrogen-enriched methane in a lean pre-mixed swirler," Office of Energy Efficiency & Renewable Energy, Livermore, 2001.
[19]. Institut fur Technische Verbrennung, "The Turbulent Burning Velocity," 28 06 2013. [Online]. Available: http://www.cce.tsinghua.edu.cn/sites/default/files/u9/Lecture13%20Combustion%20Theory.pdf. [Accessed 20 03 2014].
[20]. O. Chatakonda, E. R. Hawkes, M. J. Brear, J. H. Chen, E. Knudsen and H. Pitsch, "Modeling of the wrinkling of premixed turbulent flames in the thin reaction zones regime for large eddy simulation," Center for Turbulence Research: Proceedings of the Summer Program 2010, pp. 271-281, 2010.
[21]. Fluent Inc, "Determining Turbulence Parameters," 20 09 2006. [Online].
Available: http://aerojet.engr.ucdavis.edu/fluenthelp/html/ug/node217.htm. [Accessed 20 03 2014].
[22]. M. Day, S. Tachibana, J. Bell, M. Lijewski, V. Beckner and R. K. Cheng, "A combined computational and experimental characterization of lean premixed turbulent low swirl laboratory flames," Combustion and Flame, vol. 159, no. 1, pp. 275-290, 2012.